Anode Materials

DOI: 10.1002/anie.200804355

Three-Dimensional Porous Silicon Particles for Use in High-Performance Lithium Secondary Batteries**

*Hyunjung Kim, Byunghee Han, Jaebum Choo, and Jaephil Cho**

Silicon has been investigated for use as a next-generation, high-capacity anode material as its theoretical lithium capacity of approximately 4140 mA h g^{-1} (ca. $Li_{4.4}Si$) is eleven times higher than the capacity of graphite (ca. 372 mA h g^{-1}),[1] which is currently used as an anode material. In spite of the high capacity of silicon, severe particle pulverization can be triggered by a large volume change (> 300 %) during lithium alloying (to form Li_xSi) and de-alloying (to reform Si), which results in electrically disconnected smaller particles. These disconnected particles cause a rapid decrease in cycling stability. Intense studies have focused on reducing this volume change by using composites with an inactive carbon phase to prevent the aggregation of particle growth and to act as electrically connecting media between anode particles and the current collector when the particle is pulverized.[2–11] However, these methods lead to a decrease in the charge capacity to less than 1500 mA h g^{-1} after dozens of cycles. On the other hand, control of the volume change by control of the morphology of the Si has very rarely been reported. Chan et al. have reported Si nanowires that showed a reversible capacity of approximately 2900 mA h g^{-1} at a rate of 0.05 C, which were grown on a metallic current collector.[12] However, the capacity retention at a 2 C rate was less than 50 % of the initial capacity. Ma et al. reported a first-charge capacity of 3952 mA h g^{-1} for nestlike Si particles, but the capacity retention of the particles was 36 % between 1.6 V and 0.02 V at a rate of 0.5 C after 50 cycles.[13]

Recently, Liu and co-workers demonstrated that 3D metal foam structures of Cu and Sn fabricated by using an electrochemical deposition process exhibited not only fast transport of lithium ions through the electrolyte and the electrode, but also rapid electrochemical reactions, which resulted in a high performance anode with a superior rate capability.[14–16] For instance, a Cu_6Sn_5 alloy showed a 45 % capacity retention at a 20 C cycling rate, but, because of a very thick pore wall (> 100 μm), capacity fade was pronounced after 40 cycles.[14] To date, there have been no reports of the synthesis of 3D porous Si particles, with the exception of those from the magnesiothermic reduction method.[17] Using this method, three-dimensional silica microassemblies were formed into microporous silicon replicas in a sealed steel ampoule at 650 °C by the following reaction: $2Mg + SiO_2(s) \rightarrow 2MgO(s) + Si(s)$.

Herein, we report a versatile synthetic method for the formation of 3D porous bulk Si particles by the thermal annealing and etching of physical composites obtained from butyl-capped Si gels and SiO_2 nanoparticles at 900 °C under an Ar atmosphere. Complete etching of the SiO_2 from the SiO_2/carbon-coated Si (c-Si) composite results in the retention of the remaining c-Si as a highly porous but interconnected structure, thus preserving the starting morphology. A thin pore-wall size of approximately 40 nm can accommodate large strains without pulverization, even after 100 cycles, and a maintained charge capacity of greater than 2800 mA h g^{-1} at a rate of 1 C (= 2000 mA h g^{-1}).

SEM images of the SiO_2/c-Si composites etched in HF (1 M) for 2 h show that the Si particles retained their three-dimensional morphology and show that the Si particles have many voids, like an "octopus foot" (Figure 1 a–d). Because

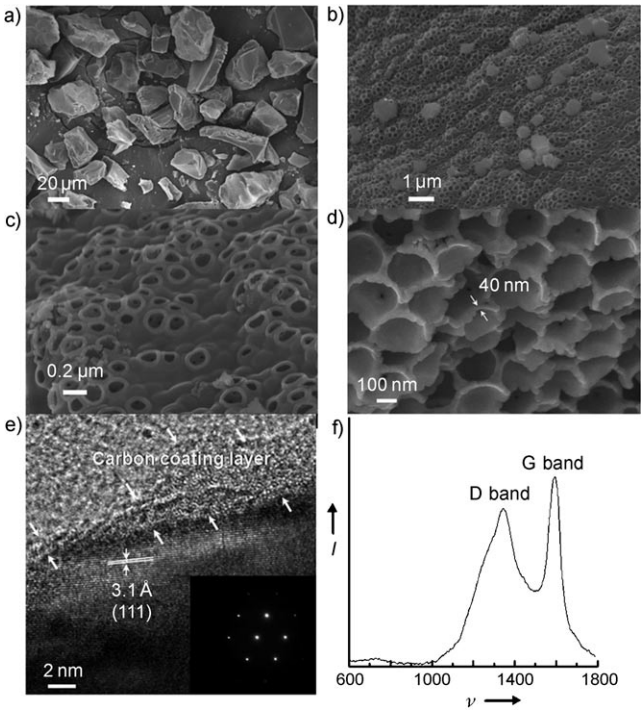

Figure 1. a), b), c), and d) SEM images of the 3D porous c-Si particles after etching ((d) is the cross-sectioned image of (e)), e) TEM image of the cross-sectioned 3D porous c-Si particle (the inset shows a selected area diffraction pattern (SADP), and f) Raman spectrum of 3D porous c-Si particles after etching. *I* = intensity.

[*] H. Kim, B. Han, Prof. J. Choo, Prof. J. Cho
Department of Applied Chemistry, Hanyang University
Ansan, 426-791 (Korea)
Fax: (+82) 31-407-3863
E-mail: jpcho@hanyang.ac.kr

[**] This work was supported by the IT R&D program of MKE/IITA (Core Lithium Secondary Battery Anode Materials for Next Generation Mobile Power Modules, 2008-F-019-01).

Supporting information for this article is available on the WWW under http://dx.doi.org/10.1002/anie.200804355.

the porous Si particles were terminated with carbon, Si dissolution by HF was unlikely to occur. After etching, interconnected SiO_2 nanoparticles were completely dissolved from the SiO_2/c-Si replica, to leave silicon with a highly porous, interconnected structure that preserved the starting particle morphology. The annealed SiO_2/c-Si composite consisted of the same particle size before and after etching. Before etching, SiO_2 nanoparticles with a size of 200 nm were embedded on the c-Si particles (Figure S1 in the Supporting Information). The cross-sectioned image of the c-Si particles shows interconnected pores with a size of 200 nm that have a wall thickness of approximately 40 nm (Figure 1 d). The specific surface area of the samples, as determined by using Brunauer–Emmett–Teller (BET) measurements, was 158 $m^2 g^{-1}$. This surface area value indicates that the silicon replicas possess a significant population of pores (Figure S2 in the Supporting Information). The XRD pattern of the porous c-Si confirms the presence of the Si phase; its crystallite size was estimated to be 100 nm (Figure S2 in the Supporting Information). X-ray photoelectron spectroscopy and energy dispersive X-ray spectroscopy (EDXS) of the porous c-Si show a minor contamination of SiO_x in the sample (Figure S2 in the Supporting Information). In the case of SiO_2, two dominant peaks at 110 and 105 eV are observed, but the peaks at 104 eV in the c-Si sample are indicative of the formation of SiO_x, where x is less than 2.[18]

The TEM image of the cross-section of the porous 3D c-Si particle shows an amorphous carbon layer with a thickness less than 10 nm (Figure 1 e). The lattice fringes of the d spacing value (3.1 Å) correspond to the (311) plane of the Si diamond cubic structure. The electron diffraction pattern of the sample shows only a spot pattern, which indicates the presence of single-crystalline Si. Raman scattering of the annealed sample was performed in order to see the ordering of the carbon layer on the sample (Figure 1 f). The two peaks at approximately 1360 and 1580 cm^{-1} are assigned to the D(disordered) band and the G(graphene) band, respectively.[19] The dimensional ratio of the D band to the G band for the samples annealed at 900 °C was estimated to be 1.51, which indicated the formation of a disordered carbon structure.

Figure 2 shows the voltage profiles of the 3D porous c-Si particles at 0.2, 0.5, 1, and 3 C rates between 1.2 V and 0 V in coin-type half cells (1 C = 2000 mA g^{-1} = 40 mA cm^{-2}). At a rate of 0.2 C, the first discharge and charge capacities are 3138 and 2820 mA g^{-1}, respectively, which indicates a coulombic efficiency of 88 %. The improved efficiency of the porous c-Si as compared to the Si nanowires (which showed ca. 79 % coulombic efficiency)[12] may be associated with the carbon coating layer, which may decrease the occurrence of side reactions with the electrolyte. Since the reversible capacity of the amorphous carbon is approximately 100 mAh g^{-1},[20] the capacity contribution from the carbon layer (12 wt %) is negligible. An estimate of the loading level of the 3D porous Si is 2.0 g cc^{-1}, therefore its volumetric density is approximately 6204 mA h cc^{-1} (2.0 g cc^{-1} × 2820 mA h g^{-1}). For comparison, the volumetric density of graphite is approximately 580 mA h cc^{-1}. The discharge capacities at a rate of 1, 2, and 3 C are 2668, 2471, 2158 mA h g^{-1}, respectively, and the capacity retention at 3 C is 72 %. This value is the highest among silicon electrodes reported to date, we believe that such a superior rate capability can be attributed to the interconnected 3D porous structure that provides fast lithium-ion mobility. Moreover, the capacity retention at a rate of 0.2 C is 99 % (282o–2780 mA h g^{-1}) after 100 cycles, while at a rate of 1 C it is 90 % (2668–2434 mA h g^{-1}). Furthermore, coulombic efficiencies of the porous c-Si particles at both 0.2 C and 1 C rates are greater than 98 %.

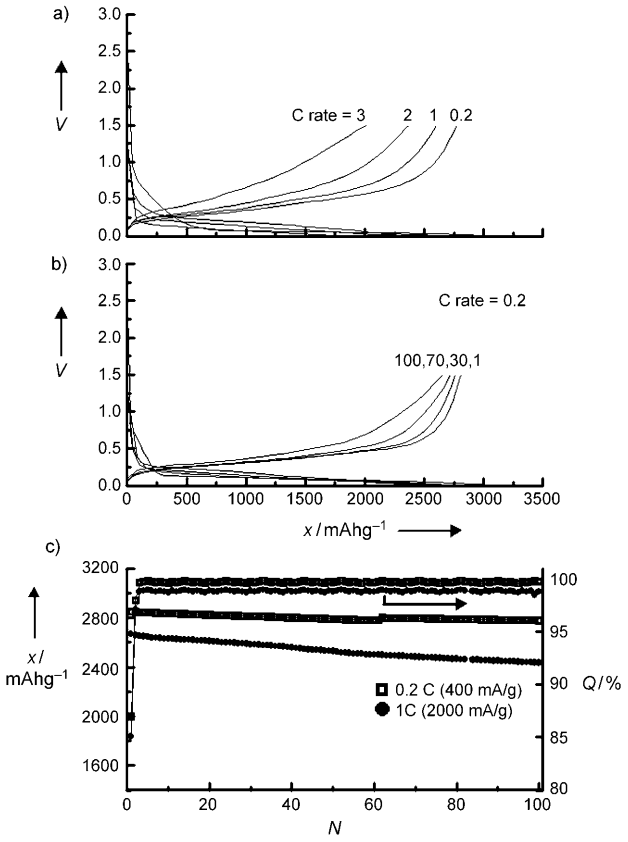

Figure 2. a) Voltage profiles of the 3D porous c-Si particles at different C rates between 0 and 1.5 V in coin-type half cells, b) voltage profiles of the 3D porous c-Si particles at a rate of 0.2 C between 0 and 1.5 V in coin-type half cells, and c) plot of charge capacities versus cycle number of the 3D porous c-Si particles cycled at different rates (0.2 C and 1 C) between 0 and 1.5 V in coin-type half cells. x = charge capacity, N = cycle number, Q = coulombic efficiency.

These capacity retentions are far superior to previously reported nanosized Si/carbon composites or Si nanoparticles.[2–13] When the bulk particles contain ordered mesopores, these pores act as a buffer layer for volume changes of the pore wall; indeed, mesoporous and crystalline tin phosphate composites showed excellent capacity retention, which demonstrates another means of controlling the volume expansion/contraction.[21–24] Although large-capacity loss after dozens of cycles was inevitable in SnO_2-based materials, well-ordered mesopores with a pore wall frame of less than 3 nm could accommodate the volume change during lithium-ion insertion and extraction, thereby demonstrating excellent cycling stability.[21–23] In this regard, pores in c-Si particles act as a "buffer layer" for alleviating the volume changes during

lithium alloying and dealloying. A study of the pore size effect on the electrochemical properties by using different SiO_2 particles is underway.

Figure 3a,b shows the SEM images of the 3D porous c-Si particles after 100 cycles. The cycled electrode exhibits similar morphology to that of the pristine sample, but a cross-sectional image shows that the pore diameter and the pore-wall thickness increased to 70 nm from 40 nm because of the volume change between the Li_xSi and Si phases. However, with a large volume change of over 300%, maintenance of such morphology is unexpected. A similar result was reported in nanowire Si with a diameter of 100 nm.[12] Figure 3d shows the XRD patterns of the 3D porous Si particles after 100 cycles, which indictates the formation of amorphous Si. It has been reported that the initial crystalline Si phase turns into amorphous Si after the initial cycles.[25,26] However, an HREM image of the cross-sectioned particle (Figure 3c) shows that crystalline Si nanoparticles less than 5 nm in diameter are distributed throughout the amorphous Si matrix. Once this amorphous Si matrix is formed, it also serves as a buffer layer for the volume changes. The crystallite size in the cycled sample decreased from 100 nm to 2–5 nm. This result indicates that the pristine Si crystalline phase is not fully transformed into the amorphous phase even after extensive cycling.

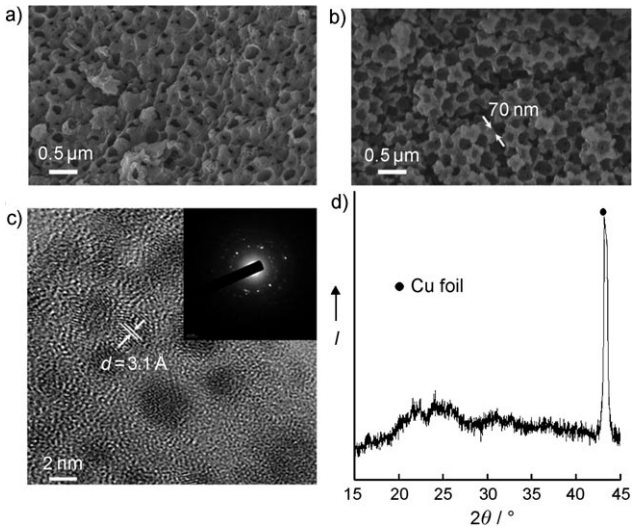

Figure 3. a) and b) Ex situ SEM images of the 3D porous c-Si particles after 100 cycles ((b) is the cross-sectioned image of (a)), c) TEM image of the 3D porous c-Si particle 100 cycles (the inset shows the SADP of image (c)), and d) XRD pattern of the 3D porous c-Si particles after 100 cycles. I = intensity.

The present work demonstrates that 3D, porous Si particles that consist of bulk sizes greater than 20 μm can be prepared by simple thermal annealing of SiO_2 and butyl-capped Si particles at 900 °C under an Ar stream. Since this method does not require the use of a sealed ampoule, the reduction is easy to scale up. These particles facilitate faster transport and better intercalation kinetics of lithium ions; the ordered arrangement guarantees that a rapid charge–discharge process can be completed in a very short time, which results in a high specific capacity even with a high charge–discharge current.

Experimental Section

Butyl-capped Si gels were prepared by reduction of $SiCl_4$ with sodium naphthalide according to a published method[19,27] and form a dark-brown solution in 1,2-dimethoxyethane. $SiCl_4$ (30 g, 99.999%, Aldrich) and 1,2-dimethoxyethane (200 g) were thoroughly mixed and added into a solution of sodium naphthalide (100 g). The resulting solution was heated at reflux at 400 °C for 9 h. This solution was mixed with butyllithium (80 mL, 99%) and stirred overnight. The solvent and naphthalene were removed by using a rotary evaporator and by heating under vacuum at 120 °C, respectively, and NaCl and LiCl byproducts were removed by partitioning between excess *n*-hexane and water. The final product was a pale-yellow viscous gel, which was then mixed with spherical silica nanoparticles (Stöber silica) prepared according to a previously reported method by Philipse et al.[28] The mixed gels/SiO_2 ratio was 70:30 wt%. The mixed gels were annealed at 900 °C under an Ar stream for 3 h. The obtained powders were immersed in an HF (1M) solution for 2 h. CHN analysis also confirmed that the carbon content in the sample was 12 wt%.

The electrolyte for coin-type half cells (2016R type) was $LiPF_6$ (1.05M) with ethylene carbonate/diethylene carbonate/ethyl-methyl carbonate (EC/DEC/EMC, 30:30:40 vol%, Cheil Industries, Korea). The coin-type half cells were cycled at a rate of 0.2 C (1 C = 2000 mA g^{-1}) between 0 and 1.5 V. The electrode was composed of 3D porous Si active material (80 wt%), poly(vinylidene fluoride) binder (10 wt%), and Super P carbon black (10 wt%). The Si loading amount was 20 mg cm^{-2}. The Super P carbon black additive did not contribute to the total capacity as it acted only as a conducting agent. Typically, five coin-cells were tested to check the capacity variation at the same cycling condition; this value was less than ±5 mAh g^{-1}. XRD patterns were obtained using $Cu_{K\alpha}$ radiation at 3 kW. Delithiated Si samples were sensitive to moisture and therefore all SEM, TEM, and XRD sampling processes were carried out in a glove box filled with pure Ar. Anhydrous solvents were used for dispersing the electrode particles used for TEM sampling, and samples were prepared by the evaporation of the dispersed nanoparticles in acetone or hexane on carbon-coated copper grids. For ex situ SEM, TEM, and XRD measurements, the specimens were sealed in plastic bags within the glovebox and removed from the glovebox. The sealed bags were then placed inside a glovebag that was, in turn, sealed around the antechamber of the SEM and TEM instruments. After the glovebag was purged with high-purity Ar gas, the specimens were removed from the plastic bags and placed on the sample holder, which was then inside the antechamber. The XRD chamber was circulated with high purity Ar gas during the ex situ XRD measurements.

Raman measurements were performed using a Renishaw 2000 Raman microscope system. A Melles Griot He–Ne laser operating at $\lambda = 632.8$ nm was used as the excitation source with a laser power of approximately 30 mW. The Rayleigh line was removed from the collected Raman scattering using a holographic notcher filter located in the collection path. Raman scattering was collected using a charge-coupled device (CCD) camera at a spectral resolution of 4 cm^{-1}. An additional CCD camera was fitted to an optical microscope to obtain optical images. Each spectrum was accumulated three times with an exposure time of 30 seconds using a 50× objective lens.

Received: September 4, 2008
Published online: November 17, 2008

Keywords: anode materials · gels · lithium · nanostructures · silicon

[1] U. Kasavajjula, C. Wang, A. J. Appleby, *J. Power Sources* **2007**, *163*, 1003.
[2] C. S. Wang, G. T. Wu, X. B. Zhang, Z. F. Qi, W. Z. Li, *J. Electrochem. Soc.* **1998**, *145*, 2751.
[3] H. Y. Lee, S. M. Lee, *Electrochem. Commun.* **2004**, *6*, 465.
[4] G. X. Wang, J. Yao, H. K. Liu, *Electrochem. Solid-State Lett.* **2004**, *7*, A250.
[5] H. Li, X. Huang, L. Chen, Z. Wu, Y. Liang, *Electrochem. Solid-State Lett.* **1999**, *2*, 547.
[6] I. S. Kim, P. N. Kumta, *J. Power Sources* **2004**, 136, 145.
[7] G. X. Wang, J. H. Ahn, J. Yao, S. Bewlay, H. K. Liu, *Electrochem. Commun.* **2004**, *6*, 689.
[8] N. Dimov, S. Kugino, M. Yoshio, *J. Power Sources* **2004**, 136, 108.
[9] Y. S. Hu, R. Demir-Cakan, M. M. Titirici, J. O. Müller, R. Schögl, M. Antonietti, J. Maier, *Angew. Chem.* **2008**, *120*, 1669; *Angew. Chem. Int. Ed.* **2008**, *47*, 1645.
[10] S. H. Ng, J. Wang, D. Wexler, K. Konstantinov, Z.-P. Guo, H. K. Liu, *Angew. Chem.* **2006**, *118*, 7050; *Angew. Chem. Int. Ed.* **2006**, *45*, 6896.
[11] M. Holzapfel, H. Buqa, W. Scheifele, P. Novák, F.-M. Petrat, *Chem. Commun.* **2005**, 1566.
[12] C. K. Chan, H. Peng, G. Liu, K. Mcilwrath, X. F. Zhang, R. A. Huggins, Y. Cui, *Nat. Nanotechnol.* **2008**, *3*, 31.
[13] H. Ma, F. Cheng, J. Chen, J. Zhao, C. Li, Z. Tao, J. Liang, *Adv. Mater.* **2007**, *19*, 4067.
[14] H.-C. Shin, J. Dong, M. Liu, *Adv. Funct. Mater.* **2005**, *15*, 582.
[15] H.-C. Shin, M. Liu, *Chem. Mater.* **2004**, *16*, 5460.
[16] H.-C. Shin, J. Dong, M. Liu, *Adv. Mater.* **2003**, *15*, 1610.
[17] Z. Bao, M. R. Weatherspoon, S. Shian, Y. Cai, P. D. Graham, S. M. Allan, G. Ahmad, M. B. Dickerson, B. C. Church, Z. Kang, H. W. Abernathy III, C. J. Summers, M. Liu, K. H. Sandhage, *Nature* **2007**, *446*, 172.
[18] H. L. Hwang, Z. Pei, H. L. Hsiao in *Handbook of Semiconductor Nanostructures and Nanodevices*, *Vol. 1* (Eds.: A. A. Balandin, K. L. Wang) American Scientific Publishers, Stevenson Ranch, CA, **2006**, Chapter 5.
[19] H. Lee, J. Cho, *Nano Lett.* **2007**, *7*, 2638.
[20] M. Noh, Y. Kown, H. Lee, J. Cho, Y. Kim, M. G. Kim, *Chem. Mater.* **2005**, *17*, 1926.
[21] E. Kim, D. Son, T.-G. Kim, J. Cho, B. Park, K. S. Ryu, S. H. Chang, *Angew. Chem.* **2004**, *116*, 6113; *Angew. Chem. Int. Ed.* **2004**, *43*, 5987.
[22] E. Kim, Y. Kim, M. G. Kim, J. Cho, *Electrochem. Solid-State Lett.* **2006**, *9*, A156.
[23] H. Kim, G. S. Park, E. Kim, S.-G. Doo, J. Cho, *J. Electrochem. Soc.* **2006**, *153*, A1633.
[24] R. Demir-Cakan, Y. S. Hu, M. Antonietti, J. Maier, M. M. Titirici, *Chem. Mater.* **2008**, *20*, 1227.
[25] Y. M. Kang, S. M. Lee, S. J. Kim, G. J. Jeong, M. S. Sung, W. U. Choi, S. S. Kim, *Electrochem. Commun.* **2007**, *9*, 959.
[26] J. Li, J. R. Dahn, *J. Electrochem. Soc.* **2007**, *154*, A156.
[27] Y. Kwon, H. Kim, S.-G. Doo, J. Cho, *Chem. Mater.* **2007**, *19*, 982.
[28] Y. Kwon, J. Cho, *Chem. Commun.* **2008**, 1109.
[29] P. Philipse, A. Vrij, *J. Colloid Interface Sci.* **1989**, *128*, 121.

